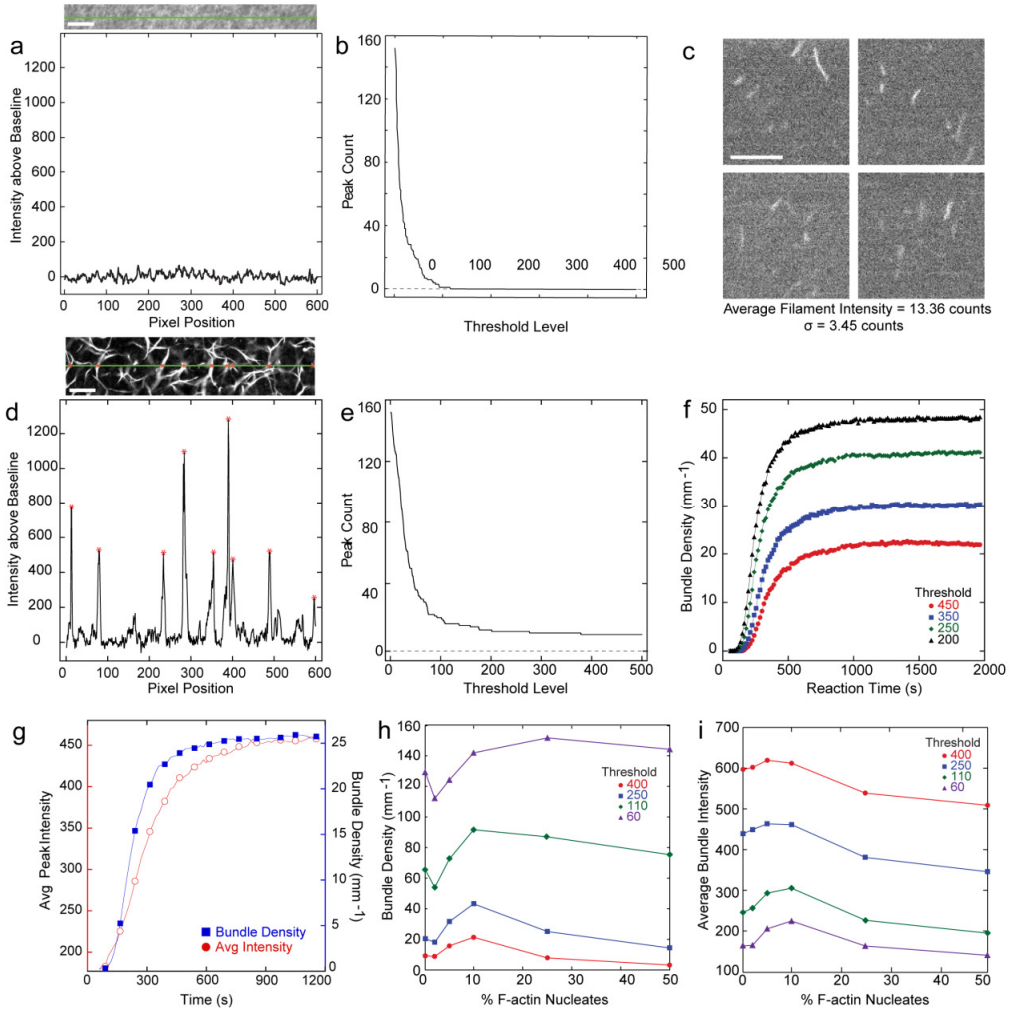

Supplementary Figure S1. Calibration of threshold peak intensity for bundle identification.
(A) (top) Fluorescent phalloidin image of 5 µM F-actin (c_α=0 µM) with representative line scan across 600 pixels (193µm, green line). (bottom) Intensity as a function of position along the line scan. (B) Histogram of the detected number of peaks along the linescan shown in part A as a function of chosen threshold level. (C) Representative confocal Images of Alexa-488 phalloidin labeled F-actin used to calculate the brightness of single actin filaments. The mean background corrected intensity of single filaments is 13.36 +/- 3.45. (D) (top) Fluorescent phalloidin image of 5µM network formed with 2µM α-actinin with representative line scan (green line), (bottom) plot of intensity along line scan and detected bundles indicated with red asterisks. Threshold intensity used to identify bundles is 200 counts above the background level (~15 filaments). (E) Histogram of the detected number of peaks along the linescan shown in part D as a function of chosen threshold level. (F) Bundle density as a function of time during the spontaneous assembly of 5 µM Actin with 2 µM α-actinin using different intensity thresholds: 200, 250, 350, and 450 counts above background (estimate bundle size of 15-33 filaments). (G) The bundle density (blue squares, right axis) and average bundle intensity (red circles, left axis) during the spontaneous assembly of 5 µM Actin with 2 µM α-actinin (data shown in Fig. 2). The bundles continue to intensify after the bundle density of the sample has saturated. (H) Steady-state bundle density for samples described in Fig. 4 using bundle thresholds of 60, 110, 250 and 400 counts above background (estimate bundle size of ~5-30 filaments). For lower thresholds which detect presence of thinner bundles and inhomogeneities in actin density, the peak is a bit less robust, indicating the presence of thinner bundles. (I) The average bundle intensity for samples described in Fig. 4 as function of chosen threshold intensity. Scale bars in A, C & D = 20µm.

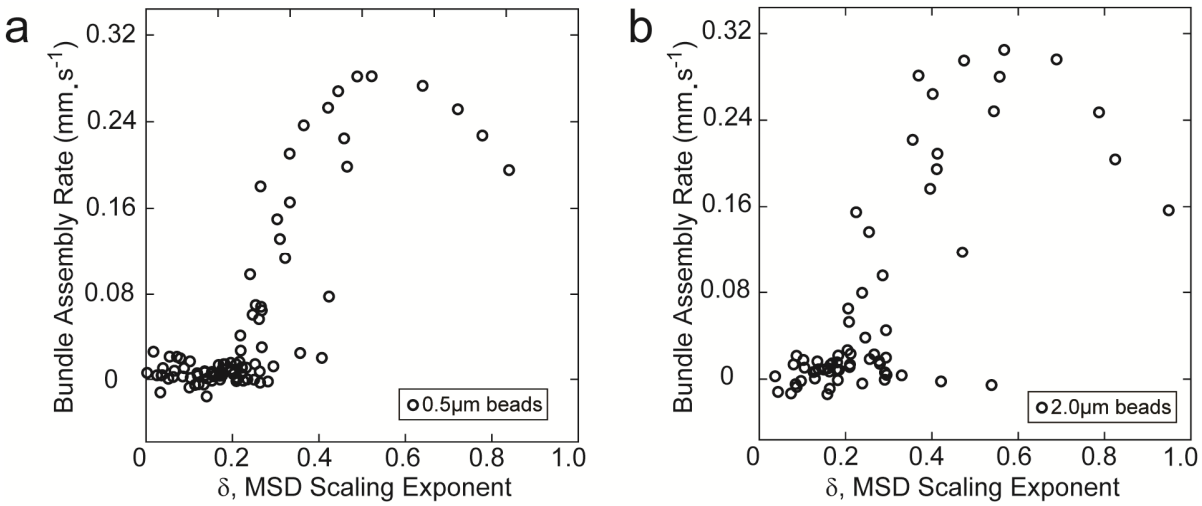

Supplementary Figure S2: MSD is independent of bead radius.
(A) 0.5μm beads and (B) 2.0μm beads embedded into an assembling 5 μM G-actin and 2 μM α-actinin network. Bundle assembly rate versus the MSD scaling exponent δ shows similar scaling between the two panels of this figure and figure 3d in regards to the trend of dropping to a rate close to zero below a MSD Scaling Exponent of around 0.5.

a

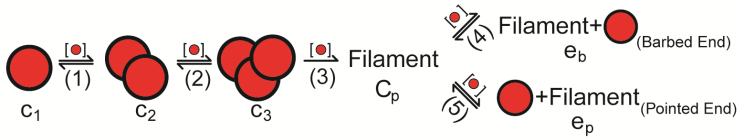

$B_1 \xrightarrow[(6)]{B_1} B_2$ $B_2 \xrightarrow[(7)]{B_1} B_3$ $B_3 \xrightarrow[(8)]{B_1} B_4$ $B_4 \xrightarrow[(9)]{B_1} B_5$ $B_5 \xrightarrow[(10)]{B_1} B_6$

$B \xrightarrow[(11)]{B_1} B_7$ $B_7 \xrightarrow[(12)]{B_1} B_8$ $B_8 \xrightarrow[(13)]{B_1} B_9$ $B_9 \xrightarrow[(14)]{B_1} B_{10}$ $B_2 \xrightarrow[(15)]{B_2} B_4$

$B_3 \xrightarrow[(16)]{B_2} B_5$ $B_4 \xrightarrow[(17)]{B_2} B_6$ $B_5 \xrightarrow[(18)]{B_2} B_7$ $B_6 \xrightarrow[(19)]{B_2} B_8$ $B_7 \xrightarrow[(20)]{B_2} B_9$

$B_8 \xrightarrow[(21)]{B_2} B_{10}$ $B_3 \xrightarrow[(22)]{B_3} B_6$ $B_4 \xrightarrow[(23)]{B_3} B_7$ $B_5 \xrightarrow[(24)]{B_3} B_8$ $B_6 \xrightarrow[(25)]{B_3} B_9$

$B_7 \xrightarrow[(26)]{B_3} B_{10}$ $B_4 \xrightarrow[(27)]{B_4} B_8$ $B_5 \xrightarrow[(28)]{B_4} B_9$ $B_6 \xrightarrow[(29)]{B_4} B_{10}$ $B_5 \xrightarrow[(30)]{B_5} B_{10}$

b

Nucleation	**Forward Rate**	**Reverse Rate**
Actin Dimer Formation, k_1(1)	35.7 $\mu M^{-1} s^{-1}$	1.63 x 10^8 s^{-1}
Actin Trimer Formation, k_2(2)	0.95 $\mu M^{-1} s^{-1}$	1300 s^{-1}
Actin Tetramer Formation, k_3(3)	4.6 $\mu M^{-1} s^{-1}$	0 s^{-1}
Elongation		
Monomer Addition to Barbed End of an Actin Filament, k_4(4)	11.6 $\mu M^{1} s^{-1}$	1.4 s^{-1}
Monomer Addition to Pointed End of an Actin Filament, k_5(5)	1.3 $\mu M^{-1} s^{-1}$	0.8 s^{-1}
Bundling		
Bundling Rate Constant, k_b (6-30)	24 $\mu M^{-2} s^{-1}$	0 $\mu M^{-1} s^{-1}$

Supplementary Figure S3. Schematic diagram and rate constants of the reactions implemented in ODE model of nucleation, elongation, and bundling of actin filaments

(A) Reaction numbers are indicated below each reaction arrow and the concentration of each reactant is identified. Red circles represent actin monomers. Reactions 1-3 depict the nucleation of actin filaments, 4 & 5 represent the elongation of actin filaments, and 6-30 represent all possible combinations of bundling filaments resulting in bundles of 10 or fewer filaments. The equations for these rate equations are discussed in the Supplemental Text. (b) The forward and reverse rate constants are indicated in this table for each kinetic rate equation that makes up our model of nucleation (Eq. a-d), elongation (Eq. e-f), and bundling (Eq. g). The corresponding reaction numbers are in parenthesis next to the description. Forward and reverse nucleation rates are based on Ref [21]. Forward rate constants for reactions 2 & 3 were decreased by 4.7 fold such that the time scale of actin assembly in the model matched that of our experiments (Fig S4). Elongation rates obtained from Ref [21]. Bundling events are treated as irreversible steps involving the coalescence of two filaments or bundles and independent of the bundle size. Details of the model are discussed in the Supplementary Text.

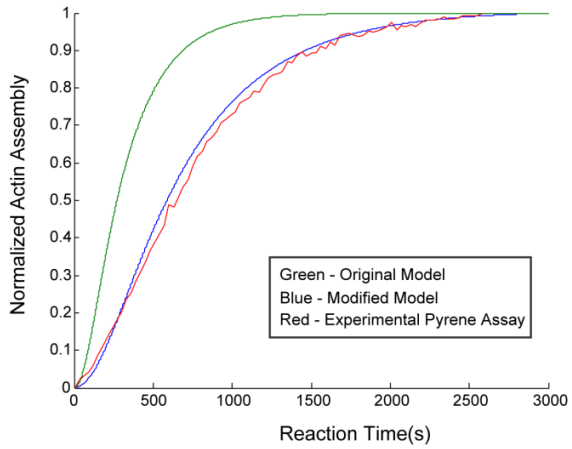

Supplementary Figure S4. Adjustment of nucleation rates to match experimental data
The change in F-actin density as a function of time during spontaneous assembly of F-actin. Experimental measurement, as measured by pyrene fluorescence and shown in Fig. 2c (red). Using published rate constants (Ref. [21]), the nucleation proceeds too quickly (green line). Reducing the nucleation rate by 4.7-fold provide a better fit to our experimental data (blue line)

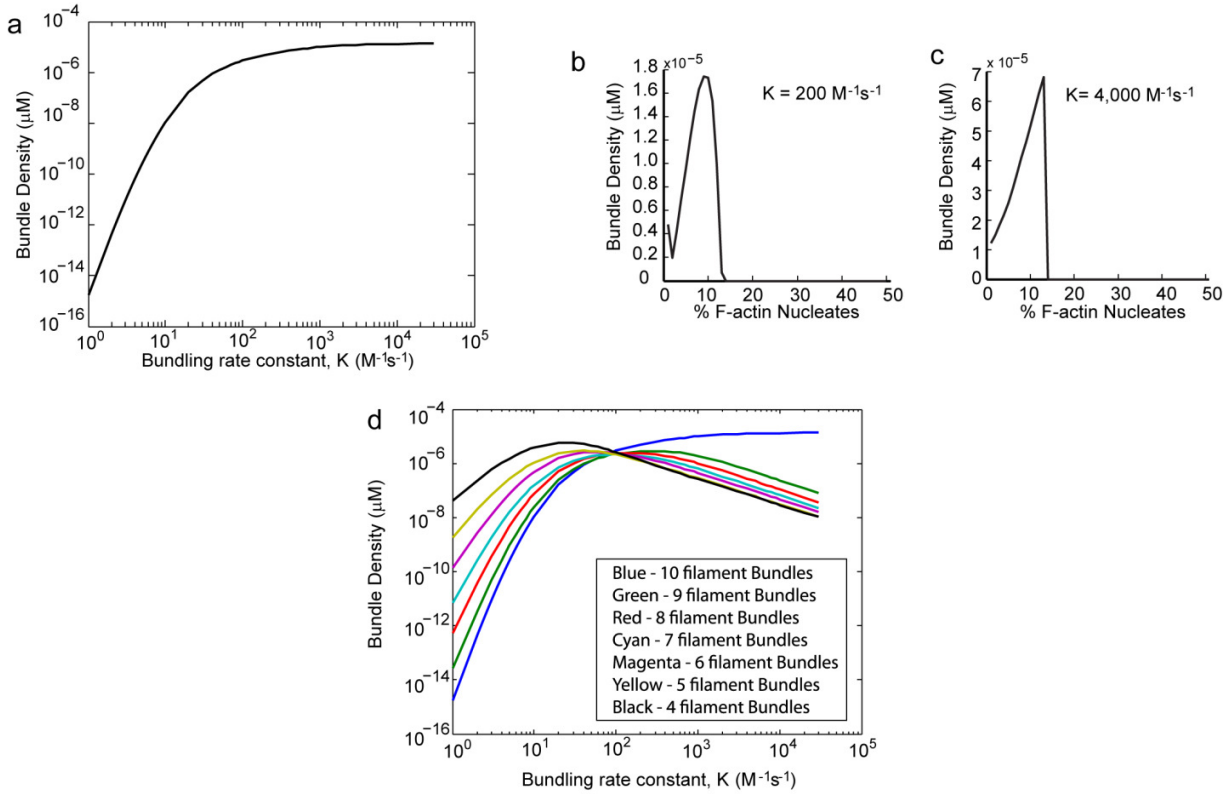

Supplementary Figure S5. Choice of bundling rate constant for simulations
(A) The steady state bundle density as a function of the bundling rate constant. (B) A non-monotonic relationship of bundle density as the fraction of F-actin nucleates is varied is insensitive to the choice of K, with the results obtained for K=200 and 4,000 M^{-1} s^{-1} shown here. (C) For our choice of K, saturation of 10-filament bundles has not occurred at steady state. Saturation does not occur until K=1,000.

Supplementary Methods

Simulation of Actin Polymerization and Bundling

We build a kinetic model to assess the polymerization and bundling dynamics of actin. Our model consists in a system of chemical rate equations for the concentration of actin monomers, oligomers, filaments and bundles. These ordinary differential equations are solved numerically. Our model comprises three interdependent sub-systems of equations accounting for F-actin nucleation, growth and bundling, which we respectively describe in Sections 1, 2 and 3. In Sec. 4, we present a heuristic criterion for entanglement in our system, which in combination with our chemical equations determines the morphology of the final bundle.

1. F-actin nucleation

F-actin nucleation is known to limit actin assembly during the spontaneous assembly of actin filament from actin monomers and has a different kinetics than the growth of long actin polymers. We thus model it by explicitly keeping track of the concentrations c_1, c_2, c_3, and C_p of actin monomers, dimers, trimers, and polymers (containing ≥ 4 monomers) respectively, an approach used previously by Paul and Pollard (Ref [21]). The corresponding rate equations are:

$$\frac{dc_1}{dt} = -2k_1^{\rightarrow}c_1c_1 - k_2^{\rightarrow}c_2c_1 - k_3^{\rightarrow}c_3c_1 + 2k_1^{\leftarrow}c_2 + k_2^{\leftarrow}c_3 + k_3^{\leftarrow}c_4 - (k_4^{\rightarrow} + k_5^{\rightarrow})C_pc_1 + (k_4^{\leftarrow} + k_5^{\leftarrow})C_p \quad \text{(a)}$$

$$\frac{dc_2}{dt} = k_1^{\rightarrow}c_1c_1 - k_1^{\leftarrow}c_2 + k_2^{\leftarrow}c_3 - k_2^{\rightarrow}c_2c_1 \quad \text{(b)}$$

$$\frac{dc_3}{dt} = k_2^{\rightarrow}c_2c_1 - k_3^{\rightarrow}c_3c_1 - k_2^{\leftarrow}c_3 \quad \text{(c)}$$

$$\frac{dC_p}{dt} = k_3^{\rightarrow}c_3c_1, \quad \text{(d)}$$

where $C_p = \sum_{n=4}^{\infty} c_n$ is the total concentration of actin polymers, with c_n denoting the concentration of F-actin n-mers. The forward and reverse rate constants for each reaction *i* are given by $k_i^{\rightarrow}$ & $k_i^{\leftarrow}$ are given in Fig. S3. The values of these rate constants are taken from Ref. 21, although $k_2^{\rightarrow}, k_3^{\rightarrow}$ are modified to match with the rate of actin assembly shown in Fig. 2E, as shown in Fig. S4. The changes in the monomer pool also reflect changes to the net growth and shrinkage of filaments which occurs at rates of $(k_4^{\rightarrow} + k_5^{\rightarrow})$ and $(k_4^{\leftarrow} + k_5^{\leftarrow})$, respectively.

The tetramer reflects the minimal stable actin filament size. Note that Eq. (a) formally allows for shrinkage of filaments of all sizes, including tetramers, which is not allowed by the reaction scheme of Fig. S3. In all calculations presented in this paper, however, the tetramer concentration is so low that this simplification does not affect the results in any noticeable way.

2. F-actin growth

We tracked net elongation of actin filaments by modeling the association and dissociation of monomers from the barbed and pointed end of actin filaments where the monomers accumulating on the barbed and pointed ends of filaments are e_b and e_p, respectively (Reactions 4 & 5 in Fig. S3).

$$\frac{de_b}{dt} = k_4^{\rightarrow}C_pc_1 + k_4^{\leftarrow}C_p$$

$$\frac{de_p}{dt} = k_5^{\rightarrow}C_pc_1 + k_5^{\leftarrow}C_p$$

The rate constants chosen were identical to those used previously by Paul and Pollard (Ref. 21) (see Fig. S3b). To determine the average length of actin polymers with $n \geq 4$ subunits, we note that the total number of actin monomers contained in these polymers is $c_{tot} - c_1 - 2c_2 - 3c_3$, where $c_{tot} = \sum_{n=1}^{\infty} nc_n$ is the total concentration of actin subunits present in our experiment. Given that the total concentration of those polymers is C_p, we can thus deduce that they each comprise $\frac{c_{tot}-c_1-2c_2-3c_3}{C_p}$ monomers on average, implying an average polymer length

$$L = d \cdot \frac{c_{tot}-c_1-2c_2-3c_3}{C_p}$$

where $d = 2.7$ nm is the length by which the polymer lengthens upon addition of an actin monomer.

To account for the presence of filament nucleates, C_p and e_b are set to non-zero initial values. The initial length of the filament nucleates is given by $d \cdot e_b(t=0)/C_p(t=0)$. The initial percentage of actin in filament nucleates is e_b/c_{tot}. The remaining actin is set to initially be as monomer. These values are set to match our experimental conditions with and without actin filament nucleates.

3. Filament bundling

We use a simplistic model of bundle assembly which ignores the spatial aspects of bundling, as well as the dependence of the bundling rate on the polymer size. We denote the concentration of bundles comprised of i filaments by B_i and keep track of concentrations of bundles up to $i_{max} = 10$ filaments (Fig. S3). We assume that any two bundles or filaments aggregate at a rate K, and take into account the constant production of new filaments through the first term of the right hand side of the following general bundling rate equation:

$$\frac{dB_i}{dt} = \delta_{i-1}\vec{k_3}c_1c_3 + \sum_{j=1}^{\lfloor i/2 \rfloor} KB_jB_{i-j} - \sum_{j=i}^{i_{max}-1} (1+\delta_{j-i})KB_iB_j$$

Where δ_i denotes the Kronecker delta ($\delta_0 = 1$ and $\delta_{i\neq 0} = 0$) and $\lfloor \dots \rfloor$ denotes the floor function. We further take into account the dependence of the bundling rate on the α-actinin concentration c_α through the simple dependence: $K = k_b \cdot c_\alpha$, where k_b is the forward rate constant for bundling reactions. This rate constant is a free parameter chosen ($k_b = 24\ M^{-2}s^{-1}$) such that the density of bundles as a function of α-actinin concentration is in qualitative agreement with our experimental data (Fig. 7F). The conclusions of our model are not dramatically impacted by changes to this rate constant (Fig. S5).

4. *Dynamic Arrest*

Introducing the total concentration of bundles $B_{tot} = \sum_{i=1}^{i_{max}} B_i$, we determine the average mesh size ξ through $\xi = B_{tot}^{-1/3}$. For the purposes of this model we implement a simple heuristic Dynamic Arrest criteria such that if $L/\xi \geq 1$, all bundling rates are set to 0. Simulations were run to 5,000s, which covered the full time of filament assembly such that *L>>ξ*.